Hydrogen Bond Dynamics in Water and Ultrafast Infrared Spectroscopy: A Theoretical Study

Klaus B. Møller,*,† Rossend Rey,‡ and James T. Hynes§,⊥

Department of Chemistry, Building 207, Technical University of Denmark, 2800 Kgs. Lyngby, Denmark, Departament de Física i Enginyeria Nuclear, Universitat Politècnica de Catalunya, Campus Nord B4-B5, Barcelona 08034, Spain, Département de Chimie, CNRS UMR 8640 PASTEUR, Ecole Normale Supérieure, 24 rue Lhomond, 75231 Paris Cedex 5, France, and Department of Chemistry and Biochemistry, University of Colorado, Boulder, Colorado 80309

Received: July 4, 2003; In Final Form: December 5, 2003

Molecular Dynamics simulations are used to examine several key aspects of recent ultrafast infrared experiments on liquid water dynamics in an amplified and extended version of a recent communication [*J. Phys. Chem. A* **2002**, *106*, 11993]. It is found that the relation between the OH stretch frequency and the length of the hydrogen bond in which the OH is involved is characterized by considerable dispersion. This dispersion, which is in part related to the varying OHO angle of the hydrogen bond, precludes a one-to-one correspondence between the OH frequency and the hydrogen bond length. Further, it is found that the time scale currently interpreted in terms of a stochastic modulation by the surrounding solvent of a highly frictionally damped hydrogen bond system is largely governed by hydrogen bond-breaking and -making dynamics, while the motion of an intact hydrogen-bonded complex is underdamped in character. A detailed analysis of these issues is provided for calculated spectral dynamics after creation of a hole in the ground vibrational state, in terms of a three time analysis (in addition to the H-bond period). Further, the validity of describing the OH frequency fluctuations as a Gaussian random process is examined, as is the character of the associated autocorrelation function of the OH frequency shift.

1. Introduction

In view of the well-recognized importance of liquid water in chemistry and physics, elucidation of its microscopic dynamics has long been of major interest. Recently, modern ultrafast spectroscopic methods have opened a new experimental window on these dynamics, and there has been intensive activity aimed at unravelling water dynamics via measurements on the experimentally convenient aqueous system of HOD diluted in D_2O, using ultrafast infrared (IR),[1−8] IR−Raman,[9] or photon echo[10,11] spectroscopy.

One major focus of these experiments has been the excited OH vibration population lifetime. This is currently interpreted as being dominated by either vibrational predissociation,[3] i.e., the breaking of the hydrogen bond (H bond) in which the excited OH stretch is involved,[12] or vibrational relaxation of the excited OH vibration without such IR-induced bond breaking.[9,13−15] A second focus, which is of interest in the present work, has concerned the spectral diffusion within the OH stretching band.[4−8] This has been initially discussed in terms of the H bond $DOH\cdots OD_2$ (hereafter OO H bond) via the time evolution of this bond initially prepared in a nonequilibrium stretched or compressed condition[5−8] and subsequently discussed more formally in terms of stochastic models which assume strongly overdamped motion of the oscillator. In the present paper, we amplify and extend the results on these spectral diffusion issues described in our recent communication.[16]

As we noted in our initial study,[16] an aspect of the initial interpretations of such experiments concerning the presumed intact OO H-bond dynamics which we found striking is that the OO motion is inferred to be overdamped: for example, an H bond initially stretched beyond its equilibrium length will, on average, monotonically relax to equilibrium, without any oscillation (see, e.g., Figure 3 of ref 5 and the discussion thereof).[17] Further, subsequent discussions all invoke a highly overdamped character of the H-bond motion.[5−8] In our view, this is surprising since the H bond is estimated in H_2O to have a reasonably high frequency of $\sim$200 cm^{-1}. This frequency has been observed in Raman spectroscopy,[18,19] IR spectroscopy,[20] and neutron scattering,[21] as well as in computer simulations of the IR spectrum.[22] To examine this issue, we performed Molecular Dynamics (MD) simulations of an equilibrium system (298 K) of an HOD molecule in liquid D_2O (simulation details are given in Section 2), focusing on the OO H-bond dynamics. Figures 1 and 2 show, both for individual trajectories and for the calculated velocity time autocorrelation, that the OO vibration is decidedly not overdamped.[23,24] In addition, Figure 2 shows the Fourier transform of the OO velocity autocorrelation, exhibiting a clear 200-cm^{-1} shoulder.

In view of the discrepancy of the evidence just recounted and any image of overdamped OO H-bond motion, it is natural to scrutinize aspects of the discussion of the experiments which may not be valid or which require clarification. In particular, we examine two key assumptions. The first is that there is a one-to-one correspondence between the frequency ω_{OH} of the OH vibration and the OO distance R in a HOD−D_2O pair. While this type of relation, in which ω_{OH} decreases with decreasing R, as the H-bond strength is increased, is quite well established

* Address correspondence to this author.
† Technical University of Denmark.
‡ Universitat Politècnica de Catalunya.
§ Ecole Normale Supérieure.
⊥ University of Colorado at Boulder.

10.1021/jp035935r CCC: $27.50
Published on Web 01/24/2004

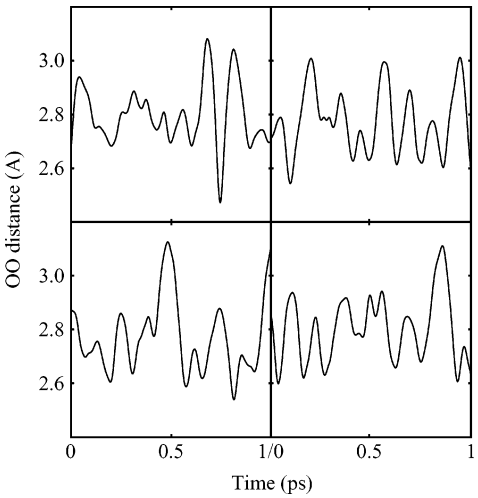

Figure 1. The OO distance $R(t)$ between HOD and a D_2O molecule initially its nearest neighbor for four arbitrarily chosen trajectories, with the condition that the two molecules remain nearest neighbors for 1 ps. The clearly underdamped motion has an amplitude of ~0.4 Å.

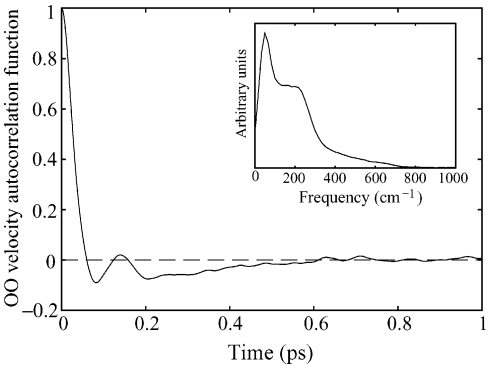

Figure 2. Normalized velocity autocorrelation function for the OO distance R between HOD and a D_2O molecule initially its nearest neighbor. Note the oscillatory behavior, with a frequency of ~200 cm^{-1}. Insert: Fourier transform of the velocity autocorrelation with a clear shoulder at ~200 cm^{-1}.

on the average for a wide variety of static systems,[25−27] it may not be sufficiently sharp to use in the context of the dynamic spectroscopic experiments.[10] The second aspect concerns the interpretation of the dynamics being probed during the experimental time window (~1−2 ps). While this has been discussed in terms of stochastic models of diffusive or high friction "Brownian oscillator" models,[5−8] it seems fair to say that a clear identification of the dynamics and measured time scales was not achieved. However, it has been noted[6,11] that the experimental time scale (~500−700 fs) is the same order of magnitude as the estimated thermal lifetime of an H bond in liquid H_2O,[28] though this was not pursued. We concluded in ref 16 that the one-to-one OH frequency H-bond length assumption is not valid, and that the observed experimental time scale should be interpreted in terms of H-bond-breaking and -making dynamics. Here we amplify and extend those results.

Several related studies by Lawrence and Skinner[29] have appeared after ref 16; we comment on the differences and similarities with ref 16 and the present work at various locations within.

The outline of the remainder of this paper is as follows. In Section 2 we give the details of the computational models and methods. The results regarding the relationship between the OH frequency and the H-bond length are presented in Section 3, and in Section 4 we present the results related to the time-resolved experiments (spectral dynamics). Some concluding remarks are given in Section 5.

2. Computational Models and Methods

In this section we present details of the MD calculations and important aspects of the calculation of the OH stretch frequency. The reader primarily interested in the results might wish to skip to Section 3 and return to Section 2 as needed.

2.1. General Simulation Details. In all of the simulations reported in this work, standard Molecular Dynamics methods[30] have been applied to a system composed of 108 water molecules. The well-known SPC/E model for intermolecular interactions and molecular geometry[31] has been adopted. No internal motions have been considered, keeping molecules rigid by way of the SHAKE[30] algorithm (that this is nonetheless consistent with the determination of the OH frequency is shown in Sections 4.3 and 4.5). The simulation box dimensions have been chosen to yield a density of 1.104 g/cm^{-1}, which corresponds to that of heavy water at ambient conditions.[32] A molecular spherical cutoff at half the box length has been used for short-range forces, while the Ewald summation procedure for the electrostatic forces has been applied. The integration algorithm is of the leapfrog type with coupling to a thermal bath,[33] with a 1 fs time step, keeping the temperature at a mean value of 298 K with a coupling constant of 0.5 ps. In all cases initial equilibration runs of 15 ps have been performed, followed by long production runs, whose length depends on the properties under study.

If not stated otherwise, the results presented within correspond to a 3-ns simulation of a single HOD molecule immersed in liquid D_2O.

2.2. Water Intramolecular Potential. The first task is the construction of a suitable intramolecular potential for HOD. The largely local nature of vibrations in the HOD molecule[13,34] allows a one-dimensional (1D) treatment of the OH coordinate as an independent vibrational mode, an approximation that is very convenient for several reasons. First, it obviously eases considerably the calculations, since the three-dimensional (3D) vibrational problem is reduced to a diatomic vibration. Second, and more importantly, this approach allows treatment of the intermolecular coupling to all orders. By contrast, taking into account the 3D nature of the HOD vibrations would require computation of the solvent−solute coupling as a power series in the normal modes,[13,35] which in conjunction with perturbational or variational calculations can be used to obtain, for instance, the instantaneous vibrational levels. The problem is that it is not possible to unambiguously ascertain if the basis set, perturbation theory level, or most remarkably the order to which the coupling is expanded is sufficient. For example, it has been shown for liquid chloroform, a liquid less associated than water, that terms up to quartic order in the coupling are required to explain the relaxation dynamics.[35]

With a 1D approach, however, such problems can be overcome, as the exact instantaneous anharmonic potential can be computed easily and solved exactly for the vibrational levels (see below). Given the large shifts characteristic of the OH stretching in liquid water, it seems essential to ensure that no important high order contributions are left out. The internal potential of Reimers and Watts,[34] which has been used here for the computation of frequency shifts, is very convenient in this connection, since it is parametrized in terms of a local (rather than normal) mode expansion. It yields the result for the gas-phase OH frequency of 3725 cm^{-1} if the other modes are frozen and the potential expanded to fourth order in the stretch

coordinate, which is acceptably close to the experimental value of 3707 cm^{-1},[36] and which highlights the small effect of intramolecular local mode coupling for HOD. This reasonably accurate result can be compared with the value of 3791 cm^{-1} obtained with the potential of Smith and Overend,[37] a potential that is expressed in terms of rectilinear normal modes rather than local modes.

It is interesting to note that perturbation theory to second order (usually employed for the intermolecular coupling) can be considerably misleading for gas-phase levels; for the Reimers and Watts potential it yields a value of 3695 cm^{-1}, a value much closer to the experimental value than the exact result, and on the opposite side. More curiously, for the Smith and Overend potential it yields 3735 cm^{-1}, much closer to experiment than the exact result obtained with this same potential. In contrast to this somewhat unpredictable character in the gas phase, perturbation theory to second order is remarkably accurate for the intermolecular induced *shift* in the liquid phase, as will be shown below. Contrary to what might be expected, this different behavior cannot be easily ascribed to a more feeble effect of intermolecular forces; actually, while the intramolecular red shift is of the order of 100 cm^{-1}, the mean intermolecular red shift is approximately 200 cm^{-1}, an interesting circumstance where intermolecular forces dominate the intramolecular forces.

2.3. Direct Calculation of the OH Frequency Shift. The solvent-induced frequency shift from the gas-phase value has been computed in two different ways. First, the vibrational problem is exactly solved in the Born−Oppenheimer (BO) approximation of a fast vibration and a slow "bath", i.e., all the other degrees of freedom, an adiabatic approximation that is reasonable given the high OH frequency (and which is also employed in the perturbational approach below). At each simulation time step, the OH vibrational coordinate q has been expanded and contracted, while the remaining degrees of freedom have been kept at their instantaneous values. For each value of q, the total energy is computed, resulting in a q-dependent perturbation which, together with the intramolecular gas-phase potential, constitutes the exact (within the BO approximation) instantaneous potential for the vibration. The resulting vibrational Schrödinger equation is then solved numerically.[38] This methodology has previously been successfully applied to the case of the cyanide ion in water.[39]

2.4. Perturbational Calculation of the OH Frequency Shift. While the method described in Section 2.3 is exact (in the adiabatic approximation), it has been demonstrated for CN^- in water[39] that a perturbational approach, if sufficiently accurate, is more useful for providing physical insight. It is therefore important to determine if such an approach holds for the present system.

The second-order perturbational calculation of the shift for a single vibrational mode in powers of the oscillator displacement results in the standard expression[40]

$$\delta\omega(t) = -\frac{3f}{\mu^2\omega_0^3}F_1(t) + \frac{1}{\mu\omega_0}F_2(t) \qquad (1)$$

involving the first (F_1) and second (F_2) derivatives of the solute−solvent potential. We have computed the instantaneous shift using this formulation, which only requires the simulation of a rigid HOD molecule immersed in the liquid. As shown in Figure 3, the agreement is extremely good; the simple and rapidly evaluated perturbational formula is very efficient at reproducing the exact results. Such a good accord is perhaps remarkable given the large shifts characteristic of the OH vibration in water, and the poor performance of second-order perturbation theory for the gas phase levels discussed in Section 2.2. Most importantly, this success allows us to use the semiclassical approach to confidently analyze the origin of the shift in detail (as was done for CN^-),[39] since the contributions resulting from different sources can be easily separated, a feature not available in a nonperturbational calculation. Two examples of such separations will be described next, while the separation central to the shift induced by any molecule of choice within the liquid will be addressed in more detail in Section 3. (This analysis is the basis of the remarks made in ref 16 concerning the role of the D_2O partner in the H bond with HOD.)

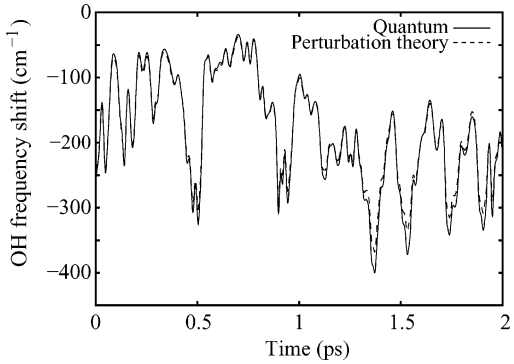

Figure 3. Comparison of the instantaneous OH frequency shift $\delta\omega(t)$ obtained by quantum mechanical calculation (see text) and by perturbation theory (eq 1), respectively.

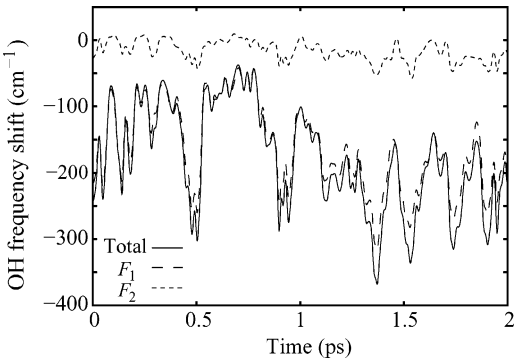

Figure 4. Contributions of the two terms in eq 1 for the OH frequency shift, involving respectively the first (F1) and second (F2) derivatives of the solute−solvent potential. The first term is clearly dominant.

2.5. Partitioning of the OH Frequency Shift According to Different Schemes. *2.5.1. Linear and Nonlinear Couplings.* According to eq 1, the simplest partition of the OH shift consists of the computation of the contributions of the linear and quadratic terms in the intermolecular coupling. Such a partition is displayed in Figure 4, from which it is evident that the quadratic contribution's weight is almost negligible. While this feature is known to apply in more simple liquids,[40,41] it is instructive to note for CN^- in water,[39] where a strong electrostatic coupling exists, that the second-order term (F_2) contribution was in fact twice that of the linear contribution. It may then be regarded as somewhat surprising that such an effect is absent for water, such that the coupling is almost linear, even though a strong coupling exists; it should be noted that the frequency shift is roughly an order of magnitude larger for OH than for CN^-. The likely explanation is that the water density around CN^- is larger than that for HOD, due to the H-bond structure disruption by the ion, which gives rise to an increased importance of repulsive interactions. In contrast, pure water is less dense and therefore repulsive interactions (which contribute particularly to the nonlinear part of the shift) are largely absent.

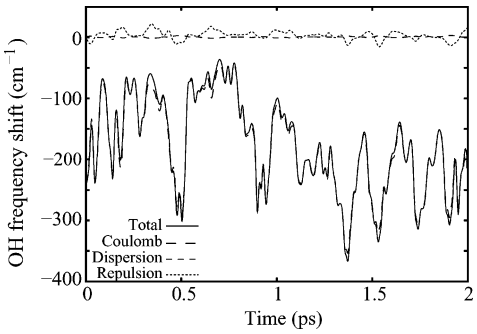

Figure 5. Contributions from various sources to the dominant F1-containing term in eq 1 for the OH frequency shift.

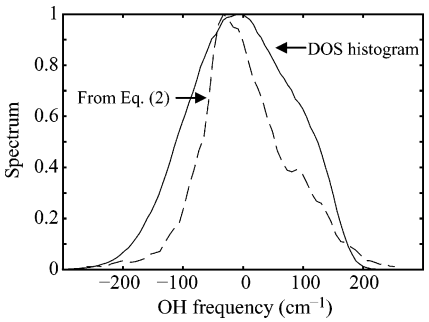

Figure 6. Density-of-states histogram $P_{eq}(\Delta\omega)$ for the OH frequency shift $\Delta\omega = \delta\omega - \langle\delta\omega\rangle$ and the spectrum $I(\Delta\omega)$ calculated according to eq 2.

This results in comparatively feeble short-range interactions (which are significantly nonlinear), in contrast with those that a charged species can induce after locally collapsing the tetrahedral water structure.[39]

2.5.2. Coulomb and Non-Coulomb Contributions. The role of Coulomb forces for solution-phase vibrational dynamics issues has been explored for several systems (see ref 42 for a review). For HOD in D_2O, it has been shown that in the dominant F_1 contribution to eq 1 for the shift, the Coulomb forces carry all the weight, with a negligible contribution of short-range forces.[42,43] Such behavior is common to all three HOD vibrational modes (OH stretch, OD stretch, HOD bend), and the considerations of Section 2.5.1 concerning this feature apply. Here such calculations have been extended to include the Coulombic nonlinear contributions (via the F_2 term in eq 1), for the particular case of the key OH mode. Figure 5 displays the contribution of each term for a short run. The inclusion of nonlinear terms does not change the picture according to which the Coulomb interactions are overwhelmingly important in water.

It is important to note that the demonstrated simultaneous dominance of Coulombic interactions and of the F_1 term in eq 1 indicate that the environmental effects on the OH stretch frequency shift are strongly related to the electric field experienced by the OH bond from all sources,[46] a perspective adopted in other contexts.[47] While we do not emphasize this aspect in our subsequent analysis of various contributions to the shift, the partitionings that we study could also be discussed in terms of the corresponding partitioning of the electric field.[48]

2.6. Total OH Frequency Shift. With the present model, the average shift induced by the solvent calculated from eq 1 is $\langle\delta\omega\rangle = -212$ cm^{-1}, giving a liquid-phase frequency of 3513 cm^{-1}, to be compared with the experimental value of 3420 cm^{-1}.[1] As a further comparison, Hermansson and co-workers,[50] using a variational approach to solve the instantaneous potential, obtained an average shift of -136 cm^{-1}, only about half of the one obtained here, the only difference from the present calculation being a different choice of model for the inter- and intramolecular potentials. Evidently, by simply changing the set of (classical) water potentials, a substantial variation in the mean shift results. If the contrary would occur, namely, that the shift is very robust, then it would make sense to try to look for the physical origin of the difference with experiment by including polarization, etc. Since, however, this is not the case, we see no real point in simply adjusting the potential in an ad hoc fashion and we do not pursue this route here.[51]

2.7. OH Spectrum. From the time series of the instantaneous OH frequency shift, we construct a density of states histogram $P_{eq}(\Delta\omega)$, where $\Delta\omega = \delta\omega - \langle\delta\omega\rangle = \omega - \langle\omega\rangle$ is the frequency shift (or frequency itself) measured with respect to its average value. The histogram is shown in Figure 6. Its fwhm is ∼240 cm^{-1}, which in principle compares very well with the experimental value[53] of 280 cm^{-1}. It is known, however, that motional narrowing is important in liquid water, and that density-of-states histograms substantially overestimate the width of the stretching band.[54] The actual spectrum, centered at the origin, is to be computed from ref 55

$$I(\Delta\omega) = \int_{-\infty}^{\infty} dt e^{i\Delta\omega t}\langle\exp[i\int_0^t d\tau\Delta\omega(\tau)]\rangle \qquad (2)$$

where $\Delta\omega(t) = \delta\omega(t) - \langle\delta\omega\rangle$ is the instantaneous shift measured with respect to its average value. The resulting spectrum is also displayed in Figure 6, and its fwhm is considerably narrower (∼130 cm^{-1}), reflecting the rapid dynamics of the solvent. We note for later reference that a "motionally narrowed" density-of-states histogram almost identical with the spectrum computed from eq 2 can be constructed using OH frequencies obtained by averaging the instantaneous OH frequencies with a time window of 200 fs (in accordance with the findings of ref 54 for this system). As for the case of the absolute value of the shift, other models may yield only half of this value,[54] and therefore this is a noticeably model-dependent property as well.

3. OH Frequency−Hydrogen Bond Length Relation

We now turn to the first of the central issues mentioned in the Introduction: the validity of the one-to-one correspondence between OH frequency and H-bond length in the context of ultrafast spectroscopy experiments on aqueous systems.

Figure 7 displays the density-of-states histogram of the OO distance and the frequency ω_{OH}, using either the instantaneous or a "motionally averaged" OH frequency obtained for each OO distance by averaging the instantaneous frequency over 200 fs as described in Section 2.7. The figure shows that there is indeed a general trend of higher frequency (smaller red shift with respect to the gas-phase value) with increasing R, consistent with weaker H bonding at larger R. However, for a given ω_{OH}, the distribution in R is quite broad, as seen clearly in Figure 8 where we plot the probability distribution in R for different ω_{OH}. The distribution is most disperse at high frequencies, for which there are more loosely H-bonded configurations (numbers based on the instantaneous OH-frequency results): at $\omega_{OH} = 3400$ cm^{-1} the fwhm in R is 0.15 Å; at $\omega_{OH} = 3600$ cm^{-1} it is 0.4 Å. Hence, in strong contrast to the standard assumption, the $\omega_{OH}-R$ relation is far from being sharply defined; indeed, on the blue side, the fwhm in R is comparable to the oscillatory OO motion amplitude (cf. Figure 1).

Here and in ref 16, while noting the existence of the average correlation, we have emphasized the departures we have found from a one-to-one $\omega_{OH}-R$ relation. In ref 29, more emphasis is

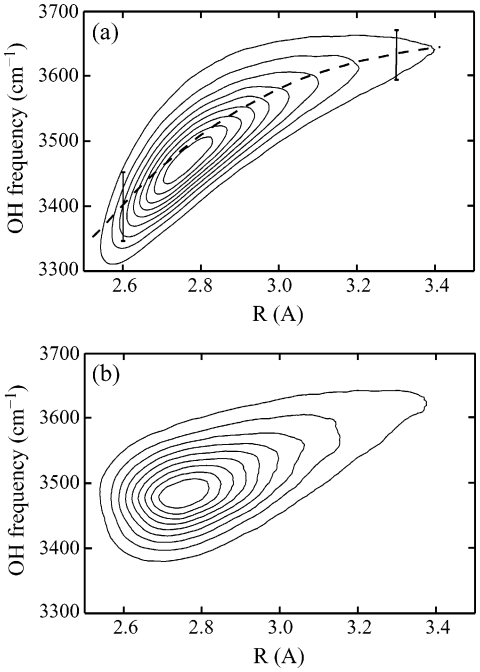

Figure 7. Density-of-states histogram for the OO distance R between HOD and its nearest neighbor and the OH frequency ω_{OH} (contour levels are 10%, 20%, ..., 90% of maximum value) using (a) the instaneous OH frequencies and (b) "motionally averaged" OH frequencies (see text). The traversing line in part a shows the average ω_{OH} for a fixed R ($\pm$ 0.01 Å) and the fwhms in ω_{OH} for $R = 2.6$ Å (200 cm^{-1}) and $R = 3.3$ Å (150 cm^{-1}), both being larger than typical experimental laser bandwidths $\sim$70 cm^{-1}.[5-7]

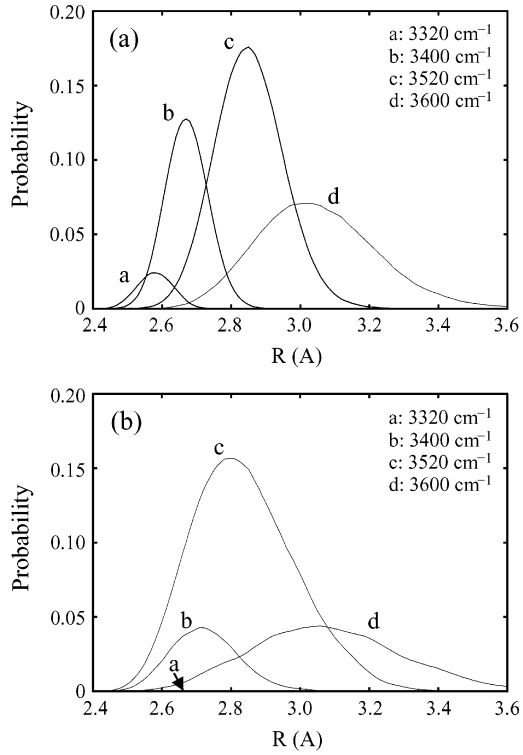

Figure 8. Probability distribution of R for fixed values of the OH frequency ($\pm$5 cm^{-1}) using (a) the instantaneous OH frequencies and (b) motionally averaged OH frequencies (see text).

placed by Lawrence and Skinner on the correlation of these quantities. Beyond our previous remarks that an assumed one-to-one correspondence indicates incorrectly that the OO H bond is overdamped, it is useful in this connection to pose a fundamental question stemming from the data above and in ref 16 in the following way: is it then correct to interpret $\omega(t)$ as a faithful record of $R(t)$, so that by monitoring the frequency one is directly monitoring the distance evolving in time? From the dispersion shown in Figure 8 the answer is negative: nothing like a uni-valued function exists.

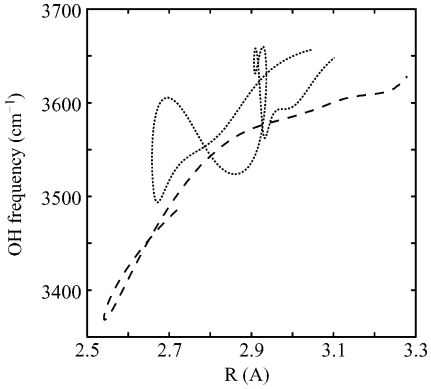

Figure 9. Examples of "trajectories" in the OH frequency−H-bond coordinate space.

It is instructive to examine real "trajectories" in the $\omega_{OH}-R$ space, sampled from the MD simulations, to make this point more clear. Figure 9 displays two such trajectories (for instantaneous frequencies), rather different in character. The dashed line represents the sort of behavior to be expected if a one-to-one correspondence would hold: it starts at a large OO separation (3.2 Å) and monotonically goes down to smaller distances, with a concomitant parallel decrease in frequency (note, however, that not even this "well-behaved" trajectory is overdamped, as it does not pause for any significant time at the most probable distance, $\sim$2.8 Å). The second trajectory (points) is more representative of the sort of wandering motion that one frequently encounters in the trajectories. Again, starting at a large OO separation ($\sim$ 3 Å) it goes down to smaller distances, but in doing so it shows rather different characteristics. Perhaps the most significant feature is the oscillatory behavior in the vertical direction displayed in different portions. The meaning of this feature is clear: for the very same OO distance, a whole range of frequencies is possible. Moreover, this range is by no means negligible: a full OH oscillation (with no change in distance) might easily span a range of more than 100 cm^{-1}. This same feature can be analyzed from a constant frequency point of view: if one imagines a horizontal line at for instance 3600 cm^{-1}, it would cross the trajectory at several points, ranging from $\sim$2.7 to $\sim$3.1 Å, i.e., one cannot predict the O−O bond length from knowledge of the frequency. Finally, it is interesting to note that the trajectory crosses itself (and the first trajectory) at several places, and at right angles: an increase in distance can imply both an increase or a decrease of frequencies, both cases with the same steepness. Again this highlights the unpredictable sequence of frequencies for a given course of H-bond separations, and vice versa.

The solid hydrate experimental data for the $\omega_{OH}-R_{eq}$ relation taken as the basis for a one-to-one relationship are in fact quite scattered,[25-27] and H-bond bending has been mentioned as a possible source of this scatter.[27] Specifically, Libowitsky[27] noted that bent H bonds yield consistently too high frequencies in the OO-distance frequency plot, pointing out that, taking into account bond symmetry, "the attractive influence of the H bond acceptor is attenuated if the H$\cdots$O distance in a bent H bond is longer (as a consequence of the bent geometry) than in a straight H bond." The possibility that the bending is an important source of the $\omega_{OH}-R$ relation dispersion we have found is explored via Figure 10, which shows the frequency distribution for a fixed

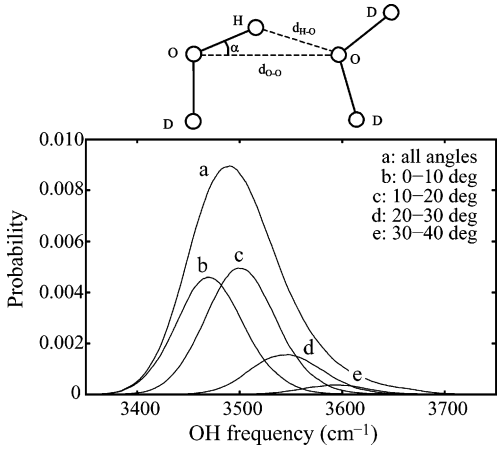

Figure 10. Probability distribution of the OH frequency for HOD−D_2O pairs with the OO distance $R = 2.8 \pm 0.01$ Å and its separation into different bending angle α intervals.

nearest-neighbor OO distance, separated into different OHO bending angle α intervals. Overall, there is a clear dependence of α on the OH frequency, with the general trend that a larger α leads to a higher ω_{OH} (smaller red shift), as expected for progressively weaker H bonds. The key lesson of Figure 10 is that the bending angle is very clearly a source of significant dispersion in the $\omega_{OH}-R$ relationship.[16] This is in accordance with the observation that most of the dispersion is already present in the frequency shift induced by just the HOD−nearest-D_2O-neighbor interaction, as now discussed.

3.1. OH Frequency Shift Induced by the Closest Molecule. The contributions of F_1 and F_2 to the OH frequency shift in eq 1 can also be split into those arising from each neighboring molecule (or even a particular site within a given molecule). Here we examine the effect of the HOD−nearest-D_2O-neighbor interaction to shed further light on the microscopic aspects of the $\omega_{OH}-R$ relationship.

First, it is found that ∼70% (146 cm^{-1}) of the total red shift is accounted for by the interaction with the molecule closest to the H in HOD. This is quite substantial (and is the basis for the remark in ref 16) and motivates a first focus, followed hereafter, on the effect of this nearest neighbor. The remaining significant influence of the rest of the molecules precludes any extreme notion according to which the H bond completely accounts for the full shift, except for small random perturbations, is not sustained by the present results.

Second, to further elucidate the OHO bending-angle α dependence of the OH frequency, we plot the values of (R,α) giving rise to a certain OH frequency. Figure 11a shows the resulting OH frequency when only including the oxygen in the neighboring D_2O molecule. These "distributions" are lines (the widths are due to a narrow frequency interval around each frequency) illustrating a one-to-one relationship between a given set (R,α) and the resulting OH frequency—which one would expect since the relative position of the oxygen neighbor to the OH bond is uniquely determined by R and α. The deviation from vertical of the line-like distributions in Figure 11a creates dispersion in the $\omega_{OH}-R$ relationship for this partial contribution. Note that this dispersion is comparable to the overall dispersion shown in Figure 10. However, this picture of the angle being responsible for the dispersion in the $\omega_{OH}-R$ relationship in a simple one-to-one fashion is somewhat obscured when making a similar plot including the contribution from the entire neighboring D_2O molecule as shown in Figure 11b. Here the "distributions" are no longer line-like (they overlap), indicating that also the orientation of the deuterium atoms on that D_2O plays a role, which is not unexpected if one considers the orientation of the electronic lone pairs of the HOD oxygen atom. This represents a topic for further research.

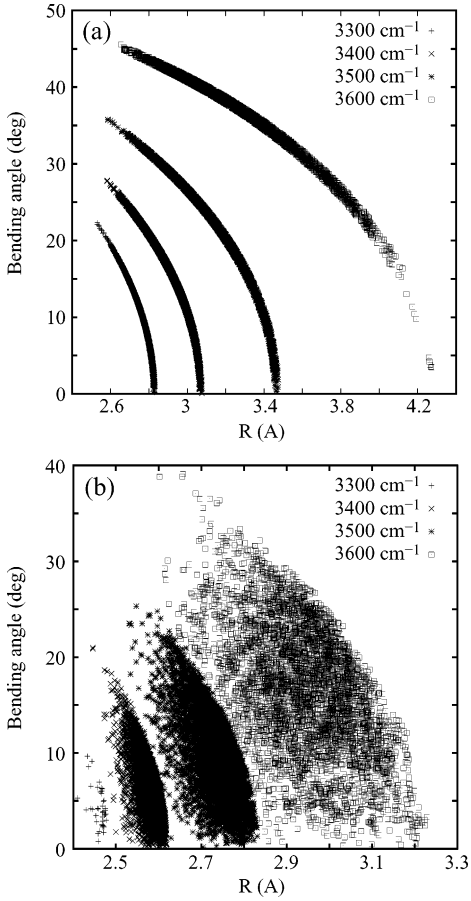

Figure 11. Pairs of oxygen−oxygen distance and bending angle (R,α) resulting in a given OH frequency (±2.5 cm^{-1}) including (a) only the nearest-oxygen contribution and (b) all nearest-D_2O contributions.

3.2. H-Bonded and Non-H-Bonded Molecules. Clearly it is of interest to analyze the OH frequency shift in terms of hydrogen bonding. A key question to answer is: What fraction of the mean shift is due to H-bonded D_2O−HOD pairs? Thus, for example, the 30% portion of the average shift noted above that does not arise from the closest molecule might be an indication that fully H-bonded molecules are after all determining the full shift, and that it is the OH stretchings which are not H bonded that can be affected by more than one neighbor. To study this possibility, all the configurations obtained from the simulation have been grouped into several classes, and the mean OH shift computed for each one separately. For this purpose, we adopt here and hereafter the geometrical definition[56] of an OO H bond in a HOD−D_2O pair: OO distance less than 3.6 Å, distance from H to O in D_2O less than 2.4 Å, and OHO bending angle α less than 30°.

The following classes have been defined, with the percentages of occurrences found noted: (a) 1 H bond: configurations in which the H in HOD is involved in a single H bond (these constitute a large majority, 87.7% of the configurations); (b) two H bonds: in some cases two D_2O molecules fulfill the hydrogen bonding conditions to a single OH bond (this occurs for a mere 0.1% of configurations); (c) partial H bonds: the angle does not fulfill the geometric conditions for hydrogen bonding (4.5% of cases), but the remaining conditions are met; (d) no H bonds: *at most* the oxygen−oxygen distance to the molecule closest to the OH fulfils the hydrogen bonding

condition (although in almost all cases the distance is larger than 3.2 Å); this is what might be taken as a "*free*" OH bond (7.7% of configurations).

An important conclusion of the above is that, although the H bond is somewhat fragile,[28] our results indicate that HOD is fully H bonded to a D_2O most of the time (~90%). (Note that this is a purely statistical statement about frequency and gives no information about the dynamical character of the H bond.) More importantly for the OH frequency shift issue, the mean red shift induced by the closest fully H-bonded molecule (class a) is 158 cm^{-1}, which is slightly larger than the total mean shift induced by the closest molecule (146 cm^{-1}) but which is far from the average value of 212 cm^{-1} for the total shift. We must conclude that for all configurations, *including* fully H-bonded pairs, there is a substantial part of the shift arising from the rest of the liquid.

Regarding the remaining classes, as is to be expected, the violation of any of the criteria (proceeding from class a to d) results in a smaller shift (higher frequency), explained by the weaker interaction. However, it is worth mentioning that for class d ("free" OH bond), the total shift (not only that of the closest molecule) is 80 cm^{-1}. This represents a substantial 40% of the total mean value (212 cm^{-1}), and is rather far from the null gas shift value that in principle might be expected in this nominally "free OH" case.

Finally, when the distribution of frequencies for fully H-bonded molecules is computed, it can be seen that a nonnegligible number of them give rise to comparable modest shifts. These results suggest that the discrete-number-of-environments picture of water,[1,2,4,10,11,57] each one characterized by a particular shift, is not an appropriate perspective.[58] However, a deeper analysis would examine how different structures are distributed in frequency space.

4. Spectral Dynamics

4.1. Hole Dynamics. We now turn to an examination of the spectral diffusion for the OH frequency. To both illustrate the impact of the $\omega_{OH}-R$ dispersion and to examine the possible role of OO H-bond-breaking and -making dynamics for ultrafast IR experiments, we calculate a quantity related to the experimental IR signal associated with the ground OH vibrational state hole dynamics, namely the time dependence of the average OH frequency $\Delta\bar{\omega}(t)$ for the distribution of OH frequencies initially created from an equilibrium distribution by excision of a band of ω_{OH} values corresponding to laser promotion to the vibrationally excited OH state. This average frequency function is closely related to the average frequency function describing the total pump−probe signal reported in refs 5 and 6. It is also directly related to the ground-state contribution to the pump−probe signal extracted from experiment in ref 7. In particular, Woutersen and Bakker[7] decompose the transient signal into bleaching of the $\nu_{OH} = 0 \rightarrow 1$ transition and $\nu_{OH} = 1 \rightarrow 2$ excited-state absorption. The bleaching consists of a hole contribution (ground state) and a particle contribution (excited state). (We also note parenthetically that the calculation of the full transient signal seems not currently possible, due to quantization requirements and the possibility of vibrational predissociation.)[3,12]

We assume that the ultrashort (pump) pulse has a Gaussian frequency profile around the center frequency ω_1, $f(\omega) = \exp[-(\omega - \omega_1)^2/(2\sigma_1^2)]$. Then, ignoring the time duration of the pulse, cross sections, etc., a hole is burned in the ground-state frequency distribution of the form (not normalized),

$$P_h(\Delta\omega,0) = P_{eq}(\Delta\omega)\exp\left[-\frac{(\Delta\omega - \Delta\omega_1)^2}{2\sigma_1^2}\right] \quad (3)$$

where $\Delta\omega_1 = \delta\omega_1 - \langle\delta\omega\rangle = \omega_1 - \langle\omega\rangle$ measures the pulse center frequency compared to the average OH frequency, such that the molecules remaining in the ground state have the (unnormalized) frequency distribution

$$P_r(\Delta\omega,0) = P_{eq}(\Delta\omega) - P_h(\Delta\omega,0) \quad (4)$$

In our simulations, we use an $f(\omega)$ with a width $\sigma_1 = 70$ cm^{-1} corresponding to the experimental value[5−7] and calculate $P_r(\Delta\omega,t)$ from a large set of system trajectories reflecting the initial distribution $P_r(\Delta\omega,0)$. The average $\Delta\omega$ of the remaining molecules is determined from

$$\Delta\bar{\omega}(t) = \frac{1}{N_r}\int d(\Delta\omega)\Delta\omega P_r(\Delta\omega,t) \quad (5)$$

where $N_r = \int d(\Delta\omega)P_r(\Delta\omega,0)$.

The obtained $\Delta\bar{\omega}(t)$ values are displayed in Figure 12 (solid curves), where we simulate excitations to the blue/red by setting $\Delta\omega_1 = \pm 100$ cm^{-1}. For the blue (red) excitation, the average frequency of the initial ensemble is less (greater) than that of the equilibrium ensemble, since more weakly (strongly) H-bonded species have been excised. As this hole is dynamically filled in with more weakly (strongly) H-bonded species, the average frequency increases (decreases). The curves in Figure 12 are normalized by their initial value. Both excitation results are mildly bimodal in time with a slightly oscillatory feature present for the latter. Analysis of these curves in terms of two exponentials yields[59] for the short time scale 66 fs (blue) and 36 fs (red) and for the long time scale 863 fs (blue) and 777 fs (red); the ratio between the short- and the long-time components is about 2:1. We have obtained similar results for other values of $\Delta\omega_1$ as well as for different choices of the laser bandwidth.

In the IR experiments, only a single longer time scale is extracted, estimated variously as 700 fs[5,6] or 500 fs,[7] this difference being related to the different experiments involved and the differing details of extraction of this time.[5−7] The short-time component as well as the slight oscillation for the red excitation result seen in Figure 12 could be quite difficult to detect due to current experimental time resolution capabilities (our simulations ignore the time duration of the laser pulse) and other contributions to the signal.[5−7] (We discuss more recent results[10,11,49,60] later in the paper.)

The fundamental interpretation of the solid curves in Figure 12 is revealed more clearly when we examine the corresponding dynamics subject to the restriction that only initially OO H-bonded molecular pairs which remain intact on the time scale of the figure are involved. Hence, we calculate the quantity

$$\Delta\bar{\omega}'(t) = \frac{1}{N_r'}\int d(\Delta\omega)\Delta\omega P_r'(\Delta\omega,t) - \langle\Delta\omega\rangle' \quad (6)$$

where $N_r' = \int d(\Delta\omega)P_r'(\Delta\omega,0)$. The prime indicates that only the above-mentioned H-bonded configurations are included in the calculation. It should be noted that the subensemble of OO H-bonded molecular pairs is no longer an equilibrium ensemble, and therefore $\langle\Delta\omega\rangle'$ is different from zero and has a slight time dependence.

The results are shown in Figure 12 (dashed curves) including only initially OO H-bonded molecular pairs which remain intact for up to 2 ps. For both excitations, the OH frequency averages in this subensemble display two important features: (i) oscil-

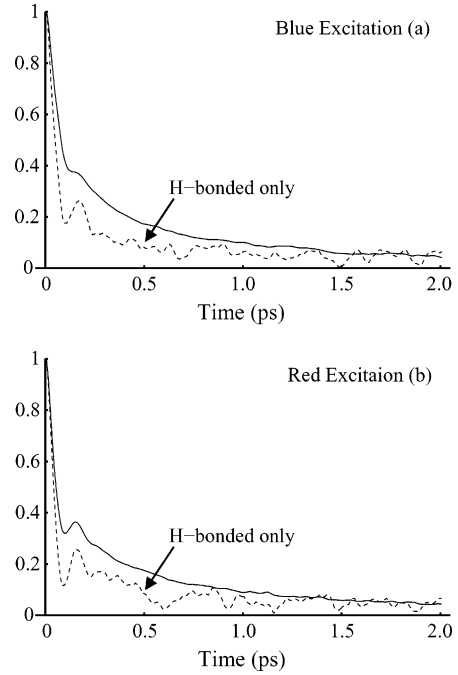

Figure 12. Solid curves: time dependence of the average OH frequency shift $\Delta\bar{\omega}_{OH}(t)$ for the distribution of OH frequencies initially created from an equilibrium distribution by excision of a band corresponding to laser promotion to the vibrationally excited OH state, calculated according to eq 5. Dashed curves: the corresponding results for subensembles containing only H-bonded HOD−D_2O pairs, calculated according to eq 6. Frames a and b are for excitation to the blue and red, respectively (see text).

latory behavior is more clearly pronounced for these intact species than for the full averages and (ii) the long-time component of the full averages has largely disappeared (it now constitutes less than 10% of the signal, compared to the about 33% it constitutes of the solid curves). Similar results are obtained when including initially OO H-bonded molecular pairs which remain intact for up to, for instance, 1.5 ps. Regarding a less critical feature, the initial values of the dashed curves compared to the solid curves, we note the following. The initial distribution of OH frequencies for the subensemble of H-bonded molecular pairs which remain intact for up to 2 ps is both narrower and red shifted compared to the equilibrium distribution of the full ensemble. Hence, for excitation to the blue, a smaller fraction of molecules is excised from the subensemble than from the full ensemble, which results in a smaller initial red shift of the dashed curve compared to the solid curve. For excitation to the red, comparable fractions of molecules are excised from the subensemble and the full ensemble, resulting in comparable initial blue shifts of the remaining molecules.

These results indicate[16] (i) that in the intact OO H-bonded species subensemble, the underdamped motion is visible, despite the $\omega_{OH}-R$ relation dispersion, a conclusion we have confirmed by calculation (see Section 4.2) of the H-bond length R dynamics in the subensemble and (ii) that the longer time dynamics in the full averages is largely determined by H-bond-breaking and -making dynamics; it is *not*, for example, determined by the overdamped motion of intact H-bonded species. Indeed, the characteristic time (∼0.5−1 ps) of the longer time component is in the range of previous estimates of the thermal lifetime of H bonds in liquid H_2O.[28] Lawrence and Skinner,[29] who estimate the HOD/D_2O H bond lifetime as ∼500 fs, have reached similar conclusions, via comparison of certain equilibrium correlation functions, although the numbers involved somewhat differ (for different HOD and D_2O models).

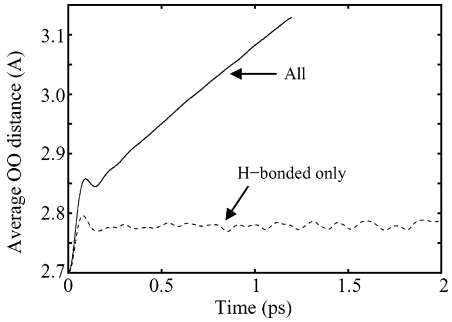

Figure 13. Average of the time-dependent OO distance $R(t)$ for an ensemble of initially H-bonded HOD−D_2O pairs with fixed initial OO distance $R(0) = 2.7 \pm 0.01$ Å (solid); average for the corresponding subensemble composed of trajectories for which the H-bonded molecular pairs remain intact for up to 2 ps (dashed). The transition to diffusive, square root in time behavior for, e.g., the "All" case is difficult to see in this figure. A separate plot (not shown) shows that the transition from linear in time to square root in time is essentially complete at ∼1 ps.

Finally, we have examined these issues by following in time the OO distance $R(t)$ for ensembles of initially H-bonded HOD−D_2O pairs with a given $R(0)$. Figure 13, for the case $R(0) = 2.7$ Å, shows the ensemble-averaged OO distance, as well as the averaged OO distance for the subensemble composed of trajectories for which the H-bonded molecular pairs remain intact for up to 2 ps. The figure clearly shows bound oscillatory behavior for the latter whereas the full-ensemble averaged OO distance shows signs of divergent, dissociating behavior—for which H-bond breaking and making is a necessary precursor, completely consistent with the picture from the hole dynamics.[61]

We also note that the averaged OO distance for the subensemble composed of trajectories for which the H-bonded molecular pairs remain intact for up to 2 ps shows no signs of diffusion toward the most probable nearest-neighbor OO distance $\langle R\rangle = 2.85$ Å, but rather oscillates steadily around the shorter distance 2.78 Å.

4.2. More Detailed Analysis of the Hole Dynamics Results. At the beginning of Section 4.1, we noted that a simple two-exponential time analysis of the hole dynamics average frequency results for blue and red excitation gives the following times: 66 and 863 fs (blue); 36 and 777 fs (red). The subsequent restriction of the trajectories to those which remain H bonded for 2 ps largely suppressed the longer time behavior. Clearly, a two-exponential fit is a very crude analysis, and, e.g., obviously misses the "bump" features at $t \sim 160$ fs in Figure 12 associated with the H-bond oscillation. Here we explore a more detailed description.

We will examine a fit of the various hole dynamics $\Delta\bar{\omega}(t)$ results via the representation

$$A\cos(\omega_{OO}t)e^{-t/\tau_1} + Be^{-t/\tau_2} + (1 - A - B)e^{-t/\tau_3} \qquad (7)$$

in which the first term is an attempt to capture the evident feature that some part of the shorter time dynamics is related to intact H-bonded species, and indeed we preassign the frequency in its oscillatory component as ω_{OO}, the H bond frequency 200 $cm^{-1} \sim 2\pi/(160\ fs) = 0.038\ fs^{-1}$. The remaining two terms, whose coefficients, together with that of the first term, provide normalization of the function, are simple exponentials, whose significance is to be determined. Equation 7 is thus a five-parameter function.

We first discuss the results of a fit of eq 7 for the time dependence of the Figure 12 average frequency results for the hole dynamics, restricted to HOD−D_2O pairs which remain

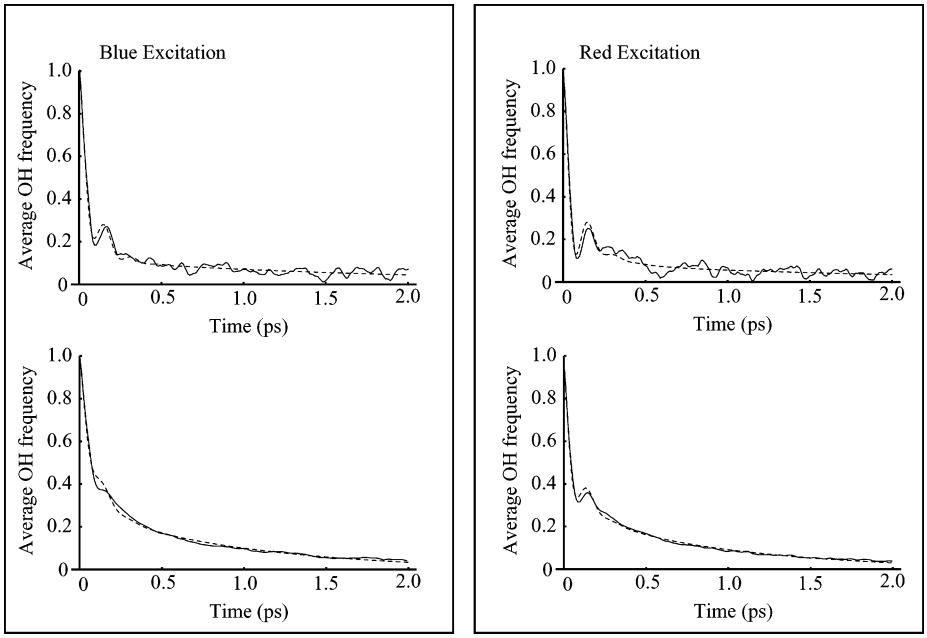

Figure 14. Fits (dashed) of the average OH frequency time dependence for the hole dynamics curves shown in Figure 12 (solid): (top) H-bond restricted; (bottom) unrestricted trajectories. These fits are reported in eqs 8 and 9, respectively, of the text.

H-bonded for 2 ps. The results of this fit for the blue and red excitation frequencies are (see Figure 14, top)

$$\text{blue:}\quad 0.31\cos(0.038t)e^{-t/97} + 0.58e^{-t/94} + 0.11e^{-t/1954}$$

$$\text{red:}\quad 0.53\cos(0.038t)e^{-t/75} + 0.39e^{-t/143} + 0.08e^{-t/2355} \quad (8)$$

(all numbers in fs), while the corresponding fits for the average frequencies for unrestricted trajectories are (see Figure 14, bottom)

$$\text{blue:}\quad 0.15\cos(0.038t)e^{-t/80} + 0.58e^{-t/100} + 0.27e^{-t/1002}$$

$$\text{red:}\quad 0.35\cos(0.038t)e^{-t/70} + 0.39e^{-t/122} + 0.26e^{-t/999} \quad (9)$$

A striking aspect to which we will return presently is the similarity of the first two terms for the restricted and unrestricted trajectory results. But first we examine the slowest decaying terms in eqs 8 and 9. We need to remark that in eq 8 for the restricted trajectories, the determination of the final terms is somewhat uncertain because the time scales obtained by the fit are similar to the time over which the curves are fitted. Nonetheless, these relatively small amplitude terms can be assigned to trajectories for which H-bond breaking and making occurs after 2 ps (recall that the restriction is to remaining H-bonded for 2 ps). The corresponding longest lived terms in the unrestricted trajectory results in eq 9 are three times larger in magnitude, and would include H-bond breaking and making at any time; the results suggest that ~1 ps is the appropriate time scale for this in the context of the hole dynamics. Although we would not wish to overemphasize it, given the overall crudeness even of eq 7 and the fact that the OH frequency is, even in the absence of dispersion, a nonlinear function of the H-bond coordinate and bend (e.g., the OH frequency is not one constant when an H bond exists and another constant when it does not), it is interesting to note this time is not far from that (1.5 ps) currently recommended as the best estimate for the time scale for H-bond making and breaking (for H_2O).[28] Finally, we should also note that the long time dependence in the H-bond restricted results, in addition to the source mentioned above, may have some contribution from the remaining solvent surrounding the HOD/D_2O pair (see Section 3.1), which judging from solvation dynamics studies in water indicating the presence of longer time scales[62] could contribute something here and to the unrestricted results.

Turning to the first two terms in eqs 8 and 9, given the similarity for restricted and unrestricted cases, and given that the times involved are noticeably shorter than any that one would connect with H-bond breaking and making and the imposed 2 ps lifetime restriction, these terms evidently represent the time behavior of the contribution of intact H-bonded species. Perhaps one should not be surprised, in view of the strong dispersion of ω_{OH}−H-bond length we have evidenced previously as well as the involvement of the bend and contributions to the frequency from the remaining solvent, that the simple first, oscillatory term by itself is insufficient to describe the intact H-bonded system.

We can add one further aspect to this analysis of the H-bond restricted hole dynamics trajectory results. In particular, we can ask if there is any *simple* relation between these results for the average frequency and the time correlation function of the fluctuation OO H-bond coordinate. We already know from our implication of the H bond-breaking and -making dynamics that the only real possibility for such a relation is for short times, and so we focus on those here. In some approaches,[57,63−65] the fluctuating OH frequency $\delta\omega$ would be linearly expanded in the H-bond coordinate and the relation would be a direct proportionality; in view of eq 1 and the fact that we have shown in Section 2.5 that the second term there is negligible, this amounts to assuming that the force on the OH coordinate is linear in the OO H-bond coordinate; again, we emphasize that given our preceding results, this could only potentially be tenable for short times.

There is, however, an important preliminary issue to address here. In the image that the H bond remains intact, the H bond time correlation function would remain bounded in time. Since, however, we have already demonstrated that H-bond-breaking and-making are important contributing processes for the OO coordinate dynamics, resulting ultimately in unbounded behavior (while the behavior of the average frequency is clearly bounded in time), we need to consider which time-correlation function definition for the H-bond coordinate could provide an appropri-

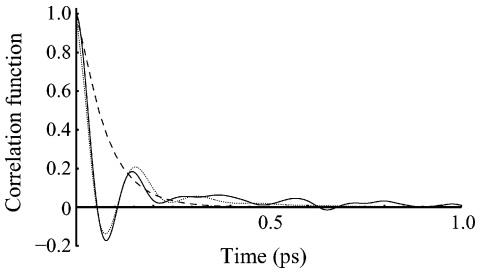

Figure 15. Oxygen−oxygen-distance autocorrelation function $C'_R(t)$ for HOD−D_2O pairs that remain H-bonded for at least 2 ps (solid). Also shown is the OO-distance autocorrelation function constructed by using the known frequency ω_{OO} of the OO vibration and a friction constant f determined from the time area of the solid line, equal to f/ω_{OO}^2, (dashed). Finally, the eq 11 fit is shown (dotted).

ate comparison. For our present purposes, we have adopted the definition

$$C'_R(t) \equiv \frac{\langle \delta R \delta R(t) \rangle'}{\langle \delta R^2 \rangle'} \tag{10}$$

where the prime notation indicates molecular pairs which are restricted to be H-bonded for 2 ps. The calculated normalized time correlation function $C'_R(t)$ is displayed in Figure 15. We pause to note that a Brownian oscillator description,[66] constructed using the known frequency ω_{OO} of the OO vibration and a friction constant f determined from the time area equal to f/ω_{OO}^2, and also shown in Figure 15, is rather a poor representation, predicting incorrectly an overdamped behavior.[67]

We compare $C'_R(t)$ with the restricted average frequency results for blue and red initial excitations, in Figure 16, and in the bottom member of each panel of this figure we also compare $C'_R(t)$ with the average OO distance for the H-bond restricted trajectories. Note that the average OO distance is measured with respect to the mean OO distance in an H-bonded pair (2.78 Å, cf. Figure 13).

There are several points to make. First, while there are certain similarities between the restricted average frequency results (for both blue and red excitations) and $C'_R(t)$, most notably in the very shortest time decay and the appearance of an OO frequency feature, there are notable deviations, e.g., $C'_R(t)$ goes negative, while the average frequency does not, and the magnitudes of the longer time tails differ. We have to conclude that there is *no* simple relation between the average frequency results and $C'_R(t)$, even for the H-bonded restricted trajectories. Second, in the bottom portion of panels a and b of Figure 16, $C'_R(t)$ is compared with the average OO separation for the H-bond restricted trajectories (normalized by its initial value), and it is seen that the correspondence of these is much closer, though some disparities remain, especially for longer times. In connection with these observations, we also note that a fit of $C'_R(t)$ with the first two functional terms of eq 7 yields (see Figure 15)

$$C'_R(t) = 0.77 \cos(0.038t)e^{-t/82} + 0.23 + e^{-t/187} \tag{11}$$

The combination of these assorted restricted trajectory results reinforces the point made above that while the H-bond restricted $C'_R(t)$ gives a quite reasonable description for the H-bond average OO separation in the hole dynamics trajectories, it is not a good description for the average frequency results, and we have indicated various sources of this disparity in our remarks above. We do notice for the two short time contributions in eqs 8 and 9 (especially for the red excitation) and eq 11 the repeated occurrence of (in addition to the H-bond period) the two time scales in the range ∼70−80 fs and ∼100−200 fs, respectively. These are times which one might associate very loosely with librational motions and (surrounding solvent molecule) OO motions, respectively.[68] However, a deeper analysis would be required to clarify any such identifications (or other ones, e.g., involving the H-bond bending or D_2O H-bond partner orientation, see Section 3.1). Instead, our fittings of various quantities have rather had the purpose of showing the OO H-bond motion explicitly and to sort out what is connected to bound H-bond motion and what is not, and to help sort out the difference between the OH frequency dynamics and features connected linearly to OO dynamics.

Before leaving the hole dynamics, we would like to emphasize a particular aspect of the above analysis, namely that even on reasonably short time scales before significant contribution of H-bond breaking and making would enter, the time behavior of the average frequencies in the hole dynamics are not well represented by a time correlation function of the H-bond coordinate. There can be many sources for this discrepancy. Beyond the dispersion in the $\omega_{OH}-R$ relationship that we have evidenced in Section 3 and in ref 16, the assumption of a linear connection between ω_{OH} and R fluctuations is quite problematical—even if one were to accept the average $\omega_{OH}-R$ relation displayed in Figure 7a—in view of the large fluctuations in the H-bond length that we have detailed within. Further, we have shown in Section 3.1 that fluctuations in the OH frequency arising from the influence of the remaining solvent molecules are not entirely negligible, a point we have discussed above in connection with the second term in our three-term representation, and which is a point that goes back to early discussions of "direct" (coupling of the OH vibration directly to the electric field of the solvent) versus "indirect" (coupling of the OH vibration to the H bond, which in turn is coupled to the solvent) mechanisms for the dephasing of H-bonded OH vibrations.[63,64] Finally, we can note that even the proper method to calculate an OO coordinate correlation function for an intact H bond can be an issue.[65]

In concluding this subsection, it is worthwhile remarking that while we certainly would not claim that the above analysis provides the last word on the key time scales involved, it is at least a refinement pointing to the need for a more detailed description beyond two simple exponentials.

4.3. The Gaussian Random Model. In this section, we comment upon the model used by Woutersen and Bakker[7] to interpret their obtained pump−probe transients within the framework of Gaussian random processes, in an effort to place our results in perspective with respect to that model and further to comment on the significance of the frequency shift autocorrelation function often used in discussions of motional narrowing[54,55,70] and in connection with the spectral diffusion problem.[7,8,10,11,57]

We first turn to the question of the Gaussian random model and consider it in connection with the hole contribution of the bleaching, as discussed in Section 4.1. In deriving an expression for this contribution, we follow the basic assumptions of ref 7 and assume that (i) the linear spectrum is Gaussian and (ii) the fluctuating frequency shift can be considered as a Gaussian random process (GRP). It is of considerable interest to examine the applicability of a GRP description in the context of our calculated hole dynamics, since its validity is by no means certain, given, e.g., the anharmonicity of the OO H bond, strongly indicated by Lippincott−Schroeder models for it,[8c12] the H-bond breaking and making dynamics we have implicated,

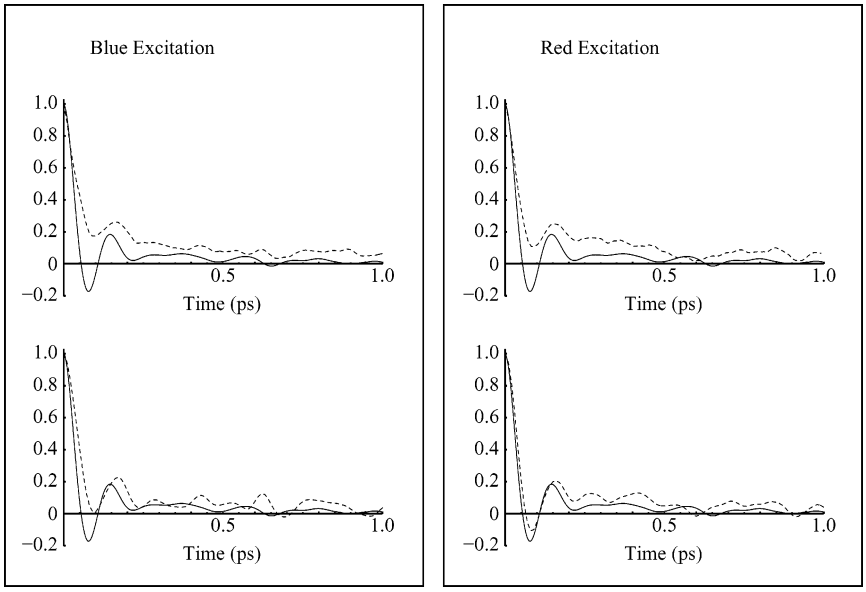

Figure 16. Comparisons of the H-bond-restricted OO separation time correlation function $C'_R(t)$ (solid) with several quantities related to the H-bond-restricted hole dynamics for blue and red excitations (dashed): (top) average OH frequency and (bottom) OO separation.

as well as the important contribution to the OH frequency shift of the nearest neighbor H-bonded D_2O and further remaining solvent contributions (cf. Section 3.1 and ref 65). It is worth observing at the outset that a GRP model for the frequency shift does not itself necessarily identify *which* molecular or individual coordinates are most important for the spectral diffusion.

To begin, by assuming that $P_{eq}(\Delta\omega)$ is Gaussian with the width σ, we obtain from eq 3 the (Gaussian) hole,

$$P_h(\Delta\omega,0) = \exp\left[-\frac{\Delta\omega_1{}^2}{2(\sigma^2+\sigma_1{}^2)}\right]\exp\left[-\frac{(\Delta\omega-\Delta\omega_0)^2}{2\sigma_0{}^2}\right] \tag{12}$$

where $\Delta\omega_0 = \Delta\omega_1\sigma^2/(\sigma^2+\sigma_1{}^2)$ and $\sigma_0{}^2 = \sigma^2\sigma_1{}^2/(\sigma^2+\sigma_1{}^2)$. Then, on the assumption that the fluctuating frequency shift can be considered as a GRP, the (normalized) frequency distribution of the hole at later times is given by ref 71

$$\hat{P}_h(\Delta\omega,t) = \left[\frac{1}{2\pi\{C^2(t)\sigma_0{}^2+\sigma^2[1-C^2(t)]\}}\right]^{-1/2} \times \exp\left[-\frac{[\Delta\omega-C(t)\Delta\omega_0]^2}{2\{C^2(t)\sigma_0{}^2+\sigma^2[1-C^2(t)]\}}\right] \tag{13}$$

where $C(t)$ is the normalized OH frequency-shift autocorrelation function,

$$C(t) = \langle\Delta\omega\Delta\omega(t)\rangle/\langle(\Delta\omega)^2\rangle \tag{14}$$

$P_h(\Delta\omega,t)$ is a Gaussian distribution at all times, which obviously approaches the equilibrium distribution $P_{eq}(\Delta\omega)$ for large times ($C_{t\to\infty}\to 0$). The center of the hole is

$$\Delta\bar{\omega}(t) = \int \mathrm{d}(\Delta\omega)\Delta\omega\hat{P}_h(\Delta\omega,t) = C(t)\Delta\omega_0 \tag{15}$$

or, equivalently, the average frequency shift at time t is

$$\delta\bar{\omega}(t) = \langle\delta\omega\rangle + C(t)(\delta\omega_0 - \langle\delta\omega\rangle) \tag{16}$$

Hence, the dynamics of the hole is given by eq 13 with the decay of the center frequency shift given by eq 16.[72] These are the expressions used by Woutersen and Bakker[7] to simulate the hole dynamics. In addition, these authors assume a single-exponential frequency-shift autocorrelation function (Markovian limit) and they determine its time constant to be 500 fs.

However, in our simulations we focus on the molecules remaining in the OH ground state with the distribution given by eq 4. Using that $\langle\Delta\omega\rangle = 0$ by construction, eq 5 can be rewritten as

$$\Delta\bar{\omega}(t) = -\frac{1}{N_r}\int \mathrm{d}(\Delta\omega)\Delta\omega P_h(\Delta\omega,t) \tag{17}$$

where $N_r = \int \mathrm{d}(\Delta\omega)P_r(\Delta\omega,0)$ and therefore within the Gaussian random model,

$$\Delta\bar{\omega}(t) = -\frac{N_h}{N_r}C(t)\Delta\omega_0 \tag{18}$$

where $N_h = \int \mathrm{d}(\Delta\omega)P_h(\Delta\omega,0)$. Thus, the time dependence of the average frequency shift's decay to its average value is again given by the frequency-shift autocorrelation. Note that $\Delta\bar{\omega}(t)$ has the opposite sign of $\Delta\omega_0$ (the laser frequency measured from the equilibrium mean OH frequency), which is natural (and we see it in our simulations), since pumping with a pulse in the red (blue) of the absorption band leaves the average frequency of the remaining molecules on the blue (red) side of the band.

To proceed further, we require the time autocorrelation function of the OH frequency shift, eq 14. This function can be calculated by using eq 1, and the result is shown in Figure 17. ($C(t)$ has also been calculated for different D_2O models by Lawrence and Skinner[29] and Fecko et al.,[49] with similar results.) Similarily to the frequency shift $\Delta\bar{\omega}(t)$, it exhibits an apparent bimodal decay; when analyzed in terms of two exponentials, we find the time constants $\tau_1 = 50$ fs and $\tau_2 = 785$ fs in a ratio of about 2:1. For comparison, we can refer to a previous calculation of frequency autocorrelation functions for the related but different case of the three normal modes of a H_2O molecule dissolved in D_2O;[74] each of these three correlation functions was found to be bimodal, with time constants of 50 and 800 fs, but in a ratio of about 1:1. While it has not been possible to resolve in IR experiments, a short-time component (30−90 fs) of the OH frequency autocorrelation has been extracted from

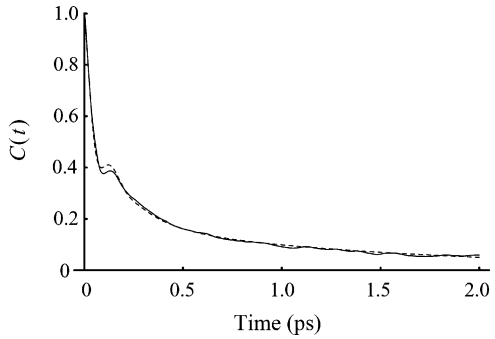

Figure 17. The OH frequency-shift autocorrelation function $C(t) = \langle \Delta\omega \Delta\omega(t) \rangle / \langle \Delta\omega^2 \rangle$. Also shown is the eq 19 fit.

an analysis of recent photon echo experiments on HOD in D_2O.[10,11] (Such a short time component in a fluctuating frequency autocorrelation function indicates a significant homogeneous broadening.[10,11])

Returning to the issue of the hole dynamics and the validity of the GRP model, our result for the OH frequency-shift autocorrelation (Figure 17) is similar to the behavior of the solid curves in Figure 12 (as noted in ref 16), although it is important to remark that the difference we observe between excitation to the blue and excitation to the red in Figure 12 cannot be accounted for by this simple analysis; this could be termed a "breakdown of the linear response approximation" by analogy to related things for solvation dynamics in electronic spectroscopy.[73] Hence, eq 18 seems capable of capturing some aspects of the simulated frequency shift's qualitative behavior. There are, however, limitations beyond the one just noted. The derivations leading to eq 18 assume that the frequency distribution of the hole as well as $P_{eq}(\Delta\omega)$ are Gaussian. Figure 6 displays $P_{eq}(\Delta\omega)$ and Figure 18 shows the calculated time-dependent frequency distribution for the remaining molecules $P_r(\Delta\omega,t)$ after excitation to the blue and the corresponding hole distribution $P_{eq}(\Delta\omega) - P_r(\Delta\omega,t)$. While $P_{eq}(\Delta\omega)$ appears reasonably Gaussian, it is not really the case that the time-dependent frequency distribution for the hole, $P_h(\Delta\omega,t)$, is Gaussian (similar results are obtained for excitation to the red). In conclusion, the very simplistic Gaussian random model provides, within the limitations noted above, a reasonably good description of the average frequency shift but *not* of the time-dependent frequency distributions themselves.[75] The clear implication is that future theoretical models must take this into account.

While we have just seen that a description in terms of the frequency shift autocorrelation function $C(t)$ has some very definite limitations, we nonetheless pursue its analysis below in an attempt to shed more light on the H-bonding dynamics.

4.4. Three Time Scale Analysis. In Section 4.1, we presented a two-exponential analysis of the hole dynamics; a similar analysis of the OH frequency shift correlation function $C(t)$ yields the times of 50 and 785 fs, respectively (see Figure 17). It is clear that this analysis is quite crude, and, for example, misses the "bump" feature at $t = 160$ fs in $C(t)$, just as the corresponding features for the hole dynamics in Figure 12 are missed. It is obviously of interest to attempt an improved representation, just as we examined in detail in Section 4.2 the hole dynamics average frequency results. Again we employ the three-term expression eq 7, and the result of the fit for $C(t)$, also shown in Figure 17, is

$$0.32 \cos(0.038t)e^{-t/60} + 0.49e^{-t/180} + 0.19e^{-t/1500} \quad (19)$$

This result should be compared with results of the fitting for the unrestricted trajectory results for the average frequency in the hole dynamics, eq 9. These are very roughly similar, especially for the red excitation result in eq 9; the three times determined in each case, while comparable, differ in detail. In view of our demonstration in Section 4.2 of the limitations of the connection between the hole dynamics and the frequency shift correlation function, this is perhaps all that could be expected.

We have carried out various analyses of $C(t)$, via its representation in eq 19, and various other quantities, e.g., the normalized time correlation function of the OO separation for H-bonded restricted trajectories, eq 10, just as we did for the hole dynamics average frequency results in Section 4.2. We do not present these here, because we consider that the hole dynamics results are a more faithful representation of the spectral dynamics than is $C(t)$. However, the overall conclusions of the $C(t)$ analyses are very similar to those of Section 4.2.[76]

4.5. Further Issues Related to the OH Frequency Shift Autocorrelation. Finally, the calculated OH frequency shift autocorrelation function $C(t)$ can be employed to address some issues connected to the overall spectrum in Figure 6. The first of these concerns the question of whether the standard cumulant expansion-based formula for the spectrum[55,70]

$$I_{cum}(\Delta\omega) = \int_{-\infty}^{\infty} dt\, e^{i\Delta\omega t} \exp[-\langle(\Delta\omega)^2\rangle \int_0^t d\tau (t-\tau) C(\tau)] \quad (20)$$

reproduces the exact eq 2 results for the spectrum. Figure 19 shows that eq 20 employing the calculated $C(t)$, Figure 17, is in fact only moderately satisfactory; a similar result is obtained by Lawrence and Skinner[29] for a different D_2O model, so that this conclusion seems to be robust. This difficulty, over and above that noted in Section 4.3 for the hole dynamics$-C(t)$ connection, makes use of $C(t)$ for the spectral dynamics problem of somewhat restricted value. Nonetheless, we will use it in the remainder of this subsection to make several general points.

First, for completeness, we have also plotted in Figure 19 two limiting approximations to the spectrum, each within the cumulant expansion-based formula eq 20. These are the Gaussian approximation obtained by ignoring the dynamics of the frequency and setting $C(t) = 1$ in eq 20, producing a purely inhomogeneously broadened spectrum and the homogeneously broadened Lorentzian approximation (or "extreme motional narrowing" limit), which involves the approximation that the time dependence of $C(t)$ is so rapid that the exponential in eq 20 can be replaced by $\exp(-t/T_2)$ with $T_2^{-1} = \langle(\Delta\omega)^2\rangle\tau_c$, where $\tau_c = \int_0^\infty dt C(t)$. As is now perhaps not so surprising, neither is a good representation either of the calculated spectrum or of the cumulant expansion-based spectrum eq 20 with use of the calculated $C(t)$,[77] and thus they do not appear to be especially useful in a discussion of the spectrum.

A final issue to be considered is the following. The calculated spectrum in Figure 6, as well as the cumulant expansion version calculated with the numerical $C(t)$ in Figure 19, shows no indication of sidebands associated with the OO H bond, i.e., features at ca. ± 200 cm^{-1}, $\pm 2 \times 200$ cm^{-1}, ..., related to the OO H bond stretch. The corresponding absence of these sidebands in experimental IR water spectra has, over the years, been used to support the overdamped character of the OO H bond dynamics.[63−65] On the other hand, we already showed in Figures 2 and 3 (see also Figure 9) that the OO H bond is not overdamped in the HOD−D_2O system. The question then is: Why are the sidebands absent? To answer this, we have examined the contributions to the spectrum eq 20 which result

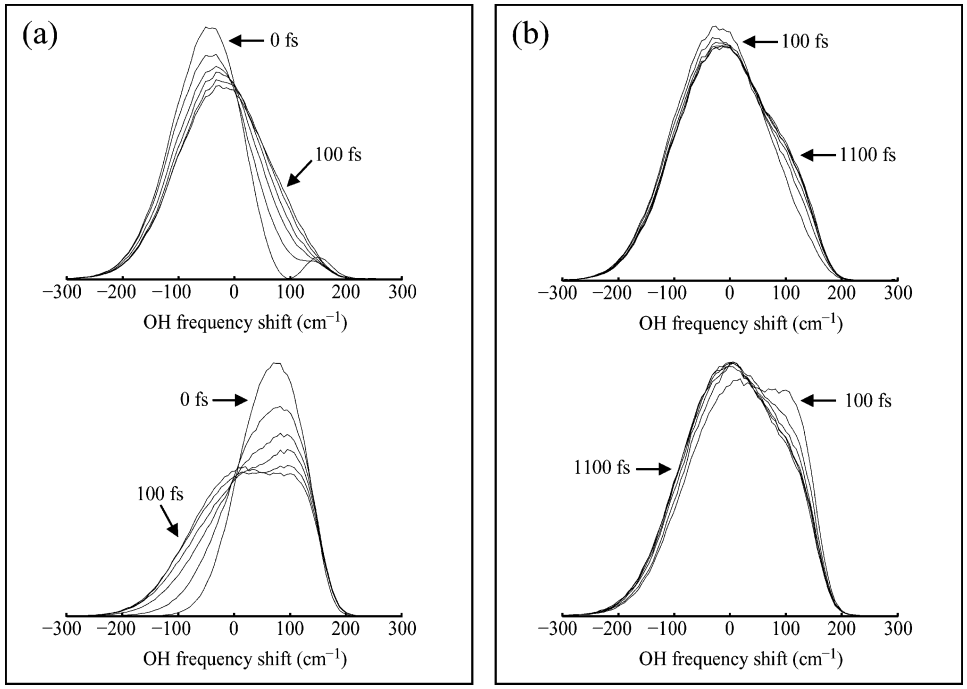

Figure 18. Calculated time-dependent frequency distribution for the remaining molecules $P_r(\Delta\omega,t)$ after excitation to the blue (top) and the corresponding hole distribution $P_{eq}(\Delta\omega) - P_r(\Delta\omega,t)$ (bottom) for times 0, 20, ..., 100 fs (a) and 100, 300, ..., 1100 fs (b).

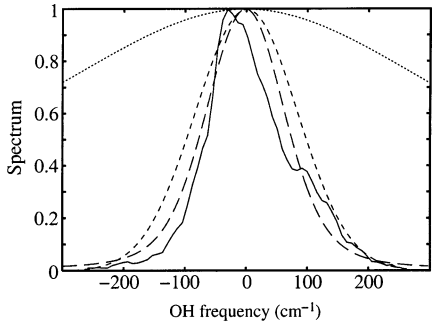

Figure 19. Various forms of the OH spectrum: the exact spectrum obtained from the standard expression eq 2 (solid), the spectrum obtained from the cumulant expansion based formula eq 20 by using the calculated OH frequency-shift autocorrelation function Figure 17 (long dashed), the Gaussian (short dashed), and the Lorenztian (dotted) limits (see text).

if $C(t)$ is approximated solely by the oscillatory term in the three-term fit in eq 19, i.e., we take $C(t) = \exp(-t/\tau_1)\cos(\omega_{OO}t)$, where $\tau_1 = 60$ fs. The reasoning here is that, with the omission of the longer time scale contributions to $C(t)$, this reference spectrum would provide the optimum opportunity for sidebands to be manifest. In particular, we examine the integral

$$I(t) = \int_0^t d\tau (t - \tau)\, C(\tau) \qquad (21)$$

This analysis gives for $I(t)$ a term linear in time as well as a remaining contribution involving OO frequency oscillations which provides the potential contribution of sidebands. Calculation shows that any oscillatory contribution to $I(t)$, and thus the spectrum, vanishes after only a few multiples of the relaxation time τ_1, whereas the linear in time term contributes, in view of its gradual annihilation of the exponential integral in eq 20, for up to times of more than $25\tau_1$. (A straightforward analytical analysis of the linear in time term in $I(t)$ gives, with $\omega_{OO}\tau_1 \sim 2$ and $\langle(\Delta\omega)^2\rangle^{1/2}\tau_1 \sim 1$, the estimate of this required time as $t \sim 5\tau_1[1 + (\omega_{OO}\tau_1)^2]/[\langle(\Delta\omega)^2\rangle\tau_1^2] \sim 25\tau_1$.) The OO oscillatory contributions to $I(t)$ are thus too quickly damped (although they are not overdamped) on the time scale of the contributing lifetime of $I(t)$ to give any sideband contribution to the spectrum.

5. Concluding Remarks

In summary, MD simulations for the HOD dilute in a liquid D_2O system have indicated very significant departures from a one-to-one correspondence between the OH vibrational frequency ω_{OH} and the OO hydrogen bond length R. Analysis shows that this dispersion is dominated by the dispersion of the H-bond OHO angle, with further contributions arising from (especially) differing OD bond orientations in the D_2O partner, and from the surrounding D_2O molecules. A related analysis fails to support the discrete number of environments picture for water.

Thus, spectroscopic selection of a given ω_{OH} value should be interpreted as providing a significant range of H-bond distances, rather than a unique one. While this feature obscures to some degree the underdamped character of the OO H-bond motion in an intact species, it does not obliterate it. More importantly, we have argued that the longer time dynamics are largely associated with the breaking and making of H bonds. (In the calculations presented, this is due to thermal motion, rather than IR-induced vibrational predissociation.[3,12,78]) Thus, for example, a spectroscopic interpretation in terms of an intact OO H-bonded species would not be appropriate. We have presented an analysis in terms of three times (in addition to the H-bond period of ~160 fs) for the calculated hole dynamics, in which the first two shorter times, approximately 70 and 100 fs, are associated with an intact H-bonded HOD/D_2O pair, while the longer time ~1 ps is strongly correlated with H bond breaking and making. As already mentioned in Section 4.1, a time roughly of order 1 ps has been previously extracted from experiments.[5−7] More recently, in photon echo experiments, short times of 30,[10,11] 130,[60] and 60 fs[49] have been extracted, and very recently an oscillation at 170 fs has been extracted.[49] Further, a very long time feature (~15 ps) has been experimentally extracted;[11] we have not found an analogous feature in any of our simulations.

Further, we have found that a Gaussian random process description, while having some qualitative validity for OH frequency shifts, is not adequate for a description of the time evolution of distributions of the OH frequency shifts. There are also certain limitations on the connection of the equilibrium frequency shift time correlation function $C(t)$ for the averaged frequency results in the hole dynamics as well as for the steady-state spectrum. While there is a broad similarity between $C(t)$ and our hole dynamics results, we believe, for the reasons mentioned within, that future efforts focused on quantities more closely connected to the experiment than is $C(t)$ could prove especially valuable. The various features mentioned above need to be taken into account in experimental interpretations, as well as in a more complete theoretical treatment, including both ground and excited OH states, currently underway. We also note that both the OH frequency dispersion as well as the time evolution of the OH frequency should be taken into account in theoretical treatments of vibrational predissociation for the OO H bond[12] and vibrational energy relaxation[13,14] as well as other aspects.[79]

We have already referred to various similarities and differences of our results and approach here and in ref 16 with that of Lawrence and Skinner[29] in various places within the present article. In a very recent contribution, Fecko et al.[49] stress an interpretation in terms of the electric field acting on the OH bond, an approach we have commented upon in Section 2.5.2. Also, rather than the focus on H-bond breaking and making, Fecko et al.[49] stress the collective aspects of the solvent motion in connection with the longer time dynamics; this is surely not orthogonal to the perspective presented in the present work (and refs 16 and 29), but the precise connection awaits elucidation. A fair summary of the theoretical and experimental situation at this point would seem to be that, while significant questions remain, important major features of the interpretation of ultrafast IR spectroscopy experiments on the HOD/D_2O system have already emerged.

The considerations related to those of the present work and ref 16 are currently being applied to the experimental results of Bakker and co-workers[80] on vibrational dynamics of water molecules in the first solvation shell of ions.

Acknowledgment. This work was supported by EC TMR network HPRN-CT-2000-19, MCYT project BFM2001-2077, the CNRS, and NSF grant CHE-0108314. K.B.M. is a Steno Fellow of the Danish Natural Science Research Council.

Note Added after ASAP Publication. This article was published ASAP on 1/24/2004 with errors in the text following eq 21 and in Figure 19. The corrected article was posted 2/03/2004.

References and Notes

(1) Graener, H.; Seifert, G.; Laubereau, A. *Phys. Rev. Lett.* **1991**, *66*, 2092.

(2) Woutersen, S.; Emmerichs, U.; Bakker, H. J. *Science* **1997**, *278*, 658.

(3) Woutersen, S.; Emmerichs, U.; Nienhuys, H.-K.; Bakker, H. J. *Phys. Rev. Lett.* **1998**, *81*, 1106. Nienhuys, H.-K.; Woutersen, S.; van Santen, R. A.; Bakker, H. J. *J. Chem. Phys.* **1999**, *111*, 1494.

(4) Laenen, R.; Rauscher, C.; Laubereau, A. *Phys. Rev. Lett.* **1998**, *80*, 2622. Laenen, R.; Rauscher, C.; Laubereau, A. *J. Phys. Chem. B* **1998**, *102*, 9304.

(5) Gale, G. M.; Gallot, G.; Hache, F.; Lascoux, N.; Bratos, S.; Leicknam, J.-C. *Phys. Rev. Lett.* **1999**, *82*, 1068.

(6) Bratos, S.; Gale, G. M.; Gallot, G.; Hache, F.; Lascoux, N.; Leicknam, J.-C. *Phys. Rev. E* **2000**, *61*, 5211.

(7) Woutersen, S.; Bakker, H. J. *Phys. Rev. Lett.* **1999**, *83*, 2077.

(8) Bakker, H. J.; Woutersen, S.; Nienhuys, H.-K. *Chem. Phys.* **2000**, *258*, 233. Gallot, G.; Lascoux, N.; Gale, G. M.; Leicknam, J.-C.; Bratos, S.; Pommeret, S. *Chem. Phys. Lett.* **2001**, *341*, 535. Bakker, H. J.; Nienhuys, H.-K.; Gallot, G.; Lascoux, N.; Gale, G. M.; Leicknam, J.-C.; Bratos, S. *J. Chem. Phys.* **2002**, *116*, 2592.

(9) Deàk, J. C.; Rhea, S. T.; Iwaki, L. K.; Dlott, D. D. *J. Phys. Chem. A* **2000**, *104*, 4866.

(10) Stenger, J.; Madsen, D.; Hamm, P.; Nibbering, E. T. J.; Elsaesser, T. *Phys. Rev. Lett.* **2001**, *87*, 027401.

(11) Stenger, J.; Madsen, D.; Hamm, P.; Nibbering, E. T. J.; Elsaesser, T. *J. Phys. Chem. A* **2002**, *106*, 2341.

(12) Staib, A.; Hynes, J. T. *Chem. Phys. Lett.* **1993**, *204*, 197.

(13) Rey, R.; Hynes, J. T. *J. Chem. Phys.* **1996**, *104*, 2356.

(14) Lawrence, C. P.; Skinner, J. L. *J. Chem. Phys.* **2002**, *117*, 5827.

(15) Experimental results in ref 3, over a temperature range including solid and liquid phases of water, were fitted to the OH frequency shift−predissociation lifetime t_{PD} formula developed in ref 12, which accounted e.g., for the lengthening time in the liquid phase with increasing temperature. The general behavior of that formula reflects the lengthening of t_{PD} with decreasing H-bond strength, within the context of the predissociation model adopted. In the alternate vibrational energy transfer mechanism developed in ref 13, the magnitude of the vibrational relaxation time t_{vib} was largely determined by the solvent-assisted energy flow between the excited OH stretch and the overtone of the HOD bend, which were 530 cm^{-1} off resonance. Although no temperature-dependent studies were done in ref 13, one can expect that t_{vib} will also increase with temperature in the liquid phase, as the H bonds in which HOD is involved weaken; this should increase the OH frequency more than the HOD frequency increasing the energy gap (the gas-phase gap between the 001 and 020 states is 925 cm^{-1}),[34] and also decrease the coupling to the solvent D_2O librations, which were implicated in the solvent assistance. Whether the resulting t_{vib}-versus-temperature behavior would provide a better fit to the data of ref 3 remains to be determined. For a general review of HOD in D_2O vibrational energy transfer, see: Rey, R.; Møller, K. B.; Hynes, J. T. *Chem. Rev.*, in press.

(16) Rey, R.; Møller, K. B.; Hynes, J. T. *J. Phys. Chem. A* **2002**, *106*, 11993.

(17) These considerations are over and above the point that the experiments of refs 5 and 6 represent average measurements, rather than, e.g., single molecule experiments.

(18) Walrafen, G. E. *J. Chem. Phys.* **1964**, *40*, 3249.

(19) Krishnamurthy, S.; Bansil, R.; Wiafe-Akenten, J. *J. Chem. Phys.* **1983**, *79*, 5863.

(20) Hasted, J. B.; Husain, S. K.; Frescura, F. A. M.; Birch, J. R. *Chem. Phys. Lett.* **1985**, *118*, 622.

(21) Chen, S.-H.; Teixeira, J. *Adv. Chem. Phys.* **1986**, *64*, 1.

(22) Souaille, M.; Smith, J. C. *Mol. Phys.* **1996**, *87*, 1333 and references therein.

(23) In this connection it is of interest to note that underdamped H-bond motion is assumed in the theoretical work of one of us on proton-transfer reactions in solution (see e.g.: Kiefer, P. M.; Hynes, J. T. *J. Phys. Chem. A* **2002**, *106*, 1850) and that oscillations have been experimentally observed for an intramolecular H bond in the following: Stenger, J.; Madsen, D.; Dreyer, J.; Nibbering, E. T. J.; Hamm, P.; Elsaesser, T. *J. Phys. Chem. A* **2001**, *105*, 2929. For a discussion of the connection of hydrogen bonding and proton transfer, see: Kiefer, P. M.; Hynes, J. T. In *Ultrafast Hydrogen Bonding Dynamics and Proton-Transfer Processes in the Condensed Phase*; Elsaesser, T., Bakker, H. J., Eds.; Kluwer: Dordrecht, The Netherlands, 2002.

(24) For reasons that will become evident in Section 4.1, we do not analyze the velocity correlation function in Figure 2 in terms of any model such as a Brownian oscillator model. We will comment on such models for a different correlation function in Section 4.2.

(25) Pimentel, G. C.; McClellan, A. L. *The Hydrogen Bond*; Freeman: San Francisco, CA, 1960.

(26) Mikenda, W. *J. Mol. Struct.* **1986**, *147*, 1. Mikenda, W.; Steinböck, S. *J. Mol. Struct.* **1996**, *384*, 159.

(27) Libowitzky, E. *Monatsh. Chem.* **1999**, *130*, 1047.

(28) Luzar, A. *J. Chem. Phys.* **2000**, *113*, 10663.

(29) Lawrence, C. P.; Skinner, J. L. *J. Chem. Phys.* **2002**, *117*, 8847. Lawrence, C. P.; Skinner, J. L. *J. Chem. Phys.* **2003**, *118*, 264. Lawrence, C. P.; Skinner, J. L. *Chem. Phys. Lett.* **2003**, *369*, 472.

(30) Allen, M. P.; Tildesley, D. J. *Computer Simulation of Liquids*; Clarendon Press: Oxford, UK, 1989.

(31) Berendsen, H.; Grigera, J.; Straatsma, T. *J. Phys. Chem.* **1987**, *91*, 6269.

(32) Lide, D. R. *CRC Handbook of Chemistry and Physics*; CRC Press: Boca Raton, FL, 1997.

(33) Berendsen, H.; Postma, J.; van Gunsteren, W.; DiNola, A.; Haak, J. *J. Chem. Phys.* **1984**, *81*, 3684.

(34) Reimers, J.; Watts, R. *Mol. Phys.* **1984**, *52*, 357.

(35) Sibert, E. L., III; Rey, R. *J. Chem. Phys.* **2002**, *116*, 237.

(36) Benedict, W. S.; Gailar, N.; Plyler, E. *J. Chem. Phys.* **1956**, *24*, 1139.

(37) Smith, D. F.; Overend, J. *Spectrochim. Acta* **1972**, *28A*, 471.
(38) Johnson, B. R. *J. Chem. Phys.* **1977**, *67*, 4086. Roemelt, J. *Chem. Phys. Lett.* **1980**, *74*, 263.
(39) Rey, R.; Hynes, J. T. *J. Chem. Phys.* **1998**, *108*, 142.
(40) Oxtoby, D. W.; Levesque, D.; Weiss, J.-J. *J. Chem. Phys.* **1978**, *68*, 5528.
(41) Laaksonen, A.; Westlund, P.-O. *Mol. Phys.* **1991**, *73*, 663.
(42) Hynes, J. T.; Rey, R. In *Ultrafast Raman and Infrared Spectroscopy*; Fayer, M., Ed.; Dekker: New York, 2001.
(43) In using this Coulombic terminology, we are of course here dealing with the given description in terms of short range and Coulombic forces, and not the more fundamental issue of the electronic character of the H bond (see e.g. refs 44 and 45 and references therein)
(44) Thompson, W. H.; Hynes, J. T. *J. Am. Chem. Soc.* **2000**, *122*, 6278.
(45) Robertson, W. H.; Johnson, M. A. *Annu. Rev. Phys. Chem.* **2003**, *54*, 173.
(46) More precisely, the appropriate combination of the electric fields at the charge sites for OH.
(47) Hermansson, K. *J. Chem. Phys.* **1991**, *95*, 3578. Hermansson, K. *J. Chem. Phys.* **1991**, *99*, 861. Hermansson, K. *Chem. Phys.* **1993**, *170*, 177. Hermansson, K. *Chem. Phys. Lett.* **1995**, *233*, 376. See also: Manca, C.; Allouche, A. *J. Chem. Phys.* **201**, *114*, 4226.
(48) Indeed, this approach has been followed in ref 49 for the frequency correlation function; we comment further on this in Sections 4.2 and 5.
(49) Fecko, C. J.; Eaves, J. D.; Loparo, J. J.; Tokmakoff, A.; Geissler, P. L. *Science* **2003**, *301*, 1698. We thank the authors for sending us a preprint of this paper, received after the work described in the present article was completed.
(50) Ojamae, L.; Hermansson, K.; Probst, M. *Chem. Phys. Lett.* **1992**, *191*, 500.
(51) In this connection, the overwhelming contribution of Coulomb forces previously discussed reinforces the idea that trying to get a better accord just by re-fitting parameters might miss substantial electronic polarization contributions. However, this cannot be easily accomplished. Polarizable models of water have been developed with a mixture of ab initio results and fittings to thermodynamical data, but they do not result in a distinctly better accord with experiment, nor do they seem to be more fundamental. In this sense calculations handling the electronic part at ab initio level[52] might constitute a better choice for a future extension, although presently they do not seem capable of providing better accord for the stretching band (for liquid D_2O, the computed band[52] is centered at ~2300 cm^{-1}, while the experimental maximum is located at ~2500 cm^{-1}).
(52) Silvestrelli, P. L.; Bernasconi, M.; Parrinello, M. *Chem. Phys. Lett.* **1997**, *277*, 478.
(53) Falk, M.; Ford, T. *Can. J. Chem.* **1966**, *44*, 1699.
(54) Ojamae, L.; Tegenfeldt, J.; Lindgren, J.; Hermansson, K. *Chem. Phys. Lett.* **1992**, *195*, 97.
(55) Oxtoby, D. W. *Adv. Chem. Phys.* **1979**, *40*, 1.
(56) Luzar, A.; Chandler, D. *J. Chem. Phys* **1993**, *98*, 8160.
(57) Georgievskii, Y.; Marcus, R. A. *J. Phys. Chem. A* **2001**, *105*, 2281.
(58) A related conclusion from a different perspective has been reached in ref 49.
(59) The numbers quoted here are slightly different from those reported in ref 16 due to a changed fitting procedure.
(60) Yeremenko, S.; Pshenichnikov, M. S.; Wiersma, D. A. *Chem. Phys. Lett.* **2003**, *269*, 107.
(61) We have also found by computation that the autocorrelation function for an initial equilibrium ensemble of $\Delta R(t) = R(t) - R_{eq}$, where R_{eq} is the equilibrium separation for an intact H-bonded species, is divergent on longer time scales for the same reason.
(62) See e.g.: Jimenez, R.; Fleming, G. R.; Kumar, P. V.; Maroncelli, M. *Nature* **1994**, *369*, 471. Horng, M. L.; Gardecki, J A.; Papazyan, A.; Maroncelli, M. *J. Phys. Chem.* **1995**, *99*, 17311.
(63) Bratos, S.; Lascombe, J.; Novak, A. In *The Hydrogen Bond*; Ratajczak, H., Orville-Thomas, W. J., Eds.; John Wiley and Sons: New York, 1980. Faniran, J. A.; Shurvell, H. F. *J. Raman Spectrosc.* **1980**, *9*, 73. Robertson, G. N.; Yarwood, J. *Chem. Phys.* **1978**, *32*, 267. Yarwood, J.; Robertson, G. N. *Chem. Phys.* **1978**, *32*, 283.
(64) Janoschek, R.; Wiedemann, E. G.; Zundel, G. *J. Chem. Soc., Faraday Trans. 2* **1973**, *69*, 505. Rösch, N.; Ratner, M. A. *J. Chem. Phys.* **1974**, *61*, 3344.
(65) Klippenstein, S. K.; Hynes, J. T. *J. Phys. Chem.* **1991**, *95*, 4651. In view of our results concerning the OO distance for H-bonded pairs in Section 4 and our remarks concerning the electric field in Section 2.5.2, a more orthogonal partitioning than was employed in this reference might prove useful.
(66) *Selected Papers on Noise and Stochastic Processes*; Wax, N., Ed.; Dover: New York, 1954. van der Zwan, G.; Hynes, J. T. *J. Phys. Chem.* **1985**, *89*, 4181. Mukamel, S. *Nonlinear Optical Spectroscopy*; Oxford University Press: New York, 1995.
(67) Interestingly, the overdamped Brownian oscillator description ($\exp[-(\omega_{OO}^2/f)t]$, not shown) is numerically very close to the full Brownian oscillator description. The conclusion is not that an overdamped description is valid, but is instead that any Brownian oscillator description for even the OO correlation function $C'_R(t)$ restricted to H-bonded pairs is invalid. We also note here that the reason that no such modeling for the OO velocity correlation function in Figure 2 was done (see ref 24) is that this function has longer time contributions from dissociating trajectories; thus, a bound oscillator should have zero time area for this correlation function, but that of Figure 2 has a finite area.
(68) For discussions of several motions in liquid D_2O, see ref 69.
(69) Martı, J.; Padró, J. A.; Gùardia, E. *Mol. Simul.* **1993**, *11*, 321. Mizoguchi, K.; Hori, A.; Tominaga, Y. *J. Chem. Phys.* **1992**, *97*, 1961.
(70) Kubo, R. In *Fluctuations, Relaxation, and Resonance in Magnetic Systems*; ter Haar, D., Ed.; Oliver and Boyd: Edinburg, 1962. Wang, C. H. *Spectroscopy of Condensed Media*; Academic Press: Orlando, FL, 1985. Morresi, A.; Mariani, L.; Distefano, M. R.; Giorgini, M. G. *J. Raman Spectrosc.* **1995**, *26*, 179.
(71) McQuarrie, D. A. *Statistical Mechanics*; Harper & Row: New York, 1976.
(72) We note that a Stokes shift of ~70 cm^{-1} has been reported in ref 7. We emphasize that we are here examining the hole dynamics governed exclusively by the ground OH vibrational state dynamics. The Stokes shift would involve investigation of the difference of the average $0 \rightarrow 1$ bleaching frequency and the $1 \rightarrow 0$ emission frequency after the pump, with the latter occurring with the vibrationally excited OH state dynamics. While one could consider assorted models for this exploiting the analogy between vibrational states and electronic states and adopting models for, e.g., different average OH dipole moments in the ground and excited vibrational states to make contact with treatments of electronic Stokes shifts,[73] we do not pursue this here.
(73) See e.g.: Carter, E. A.; Hynes, J. T. *J. Chem. Phys.* **1991**, *94*, 5961. Fonseca, T.; Ladanyi, B. M. *J. Phys. Chem.* **1991**, *95*, 2116. Fonseca, T.; Ladanyi, B. M. *J. Mol. Liq.* **1994**, *60*, 1.
(74) Diraison, M.; Guissani, Y.; Leicknam, J.-C.; Bratos, S. *Chem. Phys. Lett.* **1996**, *258*, 348.
(75) Lawrence and Skinner,[29] in an examination of the four point and two point correlation functions of the fluctuating OH frequency, conclude that while the OH frequency is not Gaussian, "this approximation could still lead to fairly accurate results".
(76) One additional type of calculation beyond those of Section 4.2 carried out is the examination of the initial Gaussian in time behavior of $C(t)$, as compared to that of the H-bond restricted OO separation correlation function eq 10. Here the Gaussian decay rate of the latter was determined from the expansion $C'_R(t) = 1 - (\eta/2)t^2 + ... \sim \exp[-(\eta/2)t^2]$ to give $\eta = \langle(\delta R)^2\rangle'/\langle\delta R^2\rangle' = (24.0\ \text{fs})^{-2}$, which is a value close to that expected (25.5 fs)$^{-2}$ for an OO frequency of 200 cm^{-1}; for comparison, a corresponding Gaussian fit to the OO velocity time correlation function in Figure 2 gives $\langle i^2\rangle/\langle v^2\rangle = (23.0\ \text{fs})^{-2}$, with a nearly perfect fit up to 70 fs. This Gaussian time behavior agrees well with the full $C'_R(t)$ for times up to 50 fs (after which $C'_R(t)$ becomes negative). This reflection of the OO frequency is, however, much muted in the behavior of $C(t)$: a Gaussian fit gives a similar initial time scale, $\langle(\delta\omega)^2\rangle/\langle\delta\omega^2\rangle = (25.1\ \text{fs})^{-2}$, but this only applies for about 15 fs, during which $C(t)$ has decayed by only about 15%.
(77) On the other hand, the Gaussian spectrum shown in Figure 19 *is* a good representation of the density-of-states histogram in Figure 6.
(78) The distinction between thermal H-bond breaking and vibrational predissociation is evidently not always appreciated.[28]
(79) Thus, attention to the various H-bonding issues discussed within might prove of value in analyzing e.g. time-dependent fluorescence solvation dynamics in aqueous systems.[62] In this connection, see also: Pimentel, G. C. *J. Am. Chem. Soc.* **1957**, *79*, 3323.
(80) Kropman, M. F.; Bakker, H. J. *Science* **2001**, *291*, 2118. Kropman, M. F.; Bakker, H. J. *J. Chem. Phys.* **2001**, *115*, 8942. Kropman, M. F.; Bakker, H. J. *Chem. Phys. Lett.* **2002**, *262*, 349. Nienhuys, H.-K.; Lock, A. J.; van Santen, R. A.; Bakker, H. J. *J. Chem. Phys.* **2002**, *117*, 8021.